

Supporting Information

for *Adv. Sci.*, DOI 10.1002/adv.202307981

Antibiotic-Induced Gut Microbiota Dysbiosis Modulates Host Transcriptome and m⁶A Epitranscriptome via Bile Acid Metabolism

Meng Yang, Xiaoqi Zheng, Jiajun Fan, Wei Cheng, Tong-Meng Yan, Yushan Lai, Nianping Zhang, Yi Lu, Jiali Qi, Zhengyi Huo, Zihe Xu, Jia Huang, Yuting Jiao, Biaodi Liu, Rui Pang, Xiang Zhong, Shi Huang, Guan-Zheng Luo, Gina Lee, Christian Jobin, A. Murat Eren, Eugene B Chang, Hong Wei, Tao Pan* and Xiaoyun Wang**

Supplementary Materials

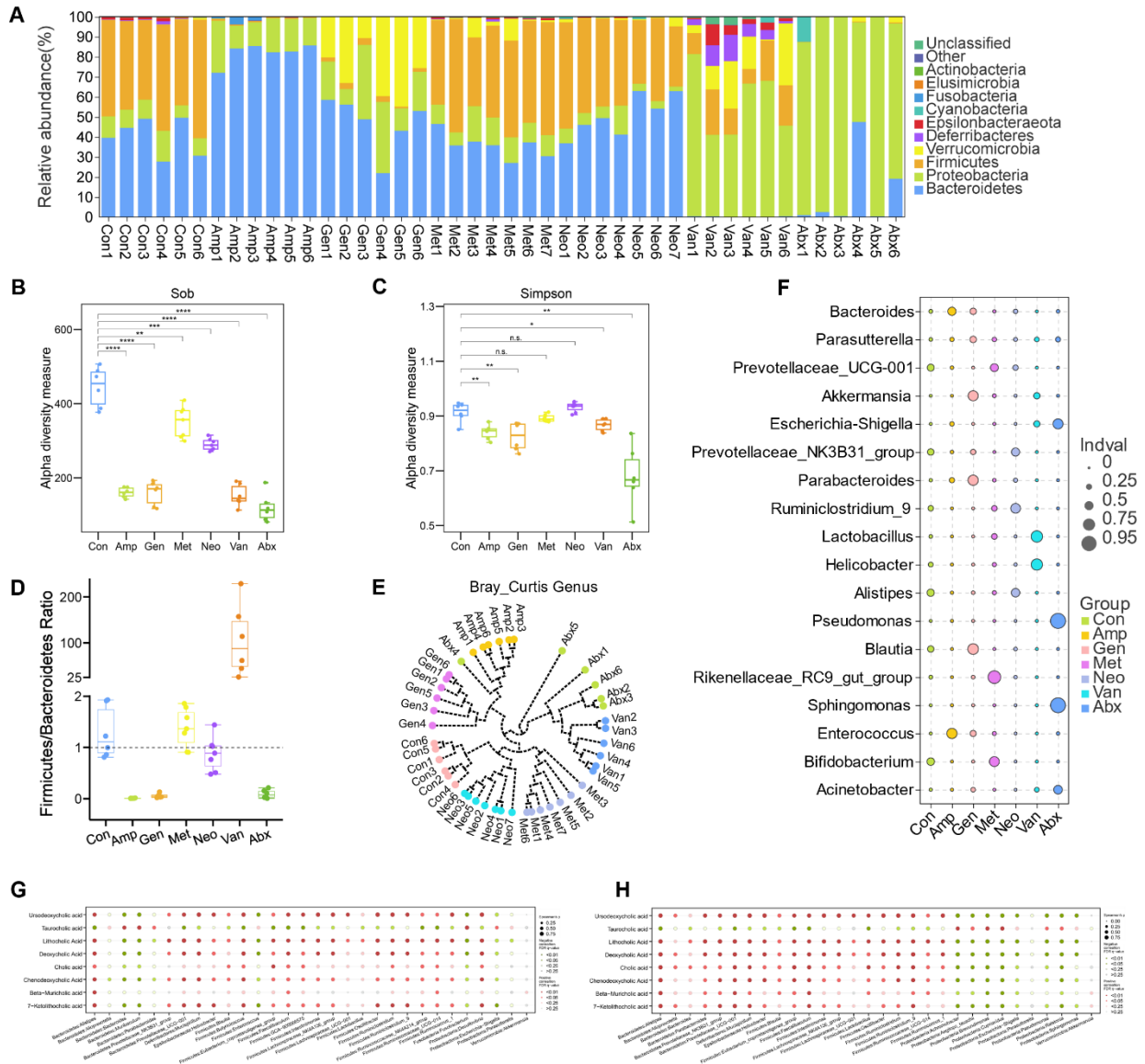


Figure S1. Microbial composition analysis of antibiotic-induced gut dysbiosis models (related to Figure 1). **(A)** Relative abundance of microbial compositions at phylum level in different antibiotic-treated groups ($n = 6-7$ each). **(B)** Sob index showing alpha-diversity of microbial compositions in different antibiotic-treated groups ($n = 6-7$ each). **(C)** Simpson index showing alpha-diversity of microbial compositions in different antibiotic-treated groups ($n = 6-7$ each). **(D)** Firmicutes/Bacteroidetes ratios in different antibiotic-treated groups ($n = 6-7$ each). **(E)** UPGMA analysis of microbial compositions at genus level in different antibiotic-treated groups ($n = 6-7$ each). **(F)** Indicator value analysis of microbial compositions at genus level in different antibiotic-treated groups ($n = 6-7$ each). **(G)** Correlation analysis of differential metabolites with the top 30 microbial compositions at genus level between Amp group and Con group ($n = 5$ each). **(H)** Correlation analysis of differential metabolites with the top 30 microbial compositions at genus level between Abx group and Con group ($n = 5$ each). Groups include control (Con), ampicillin (Amp), gentamicin (Gen), metronidazole (Met), neomycin (Neo), vancomycin (Van), antibiotic cocktail (Abx, mixture of the above five antibiotics). $*P < 0.05$, $**P < 0.01$, $***P < 0.001$, $****P < 0.0001$, Student's t test.

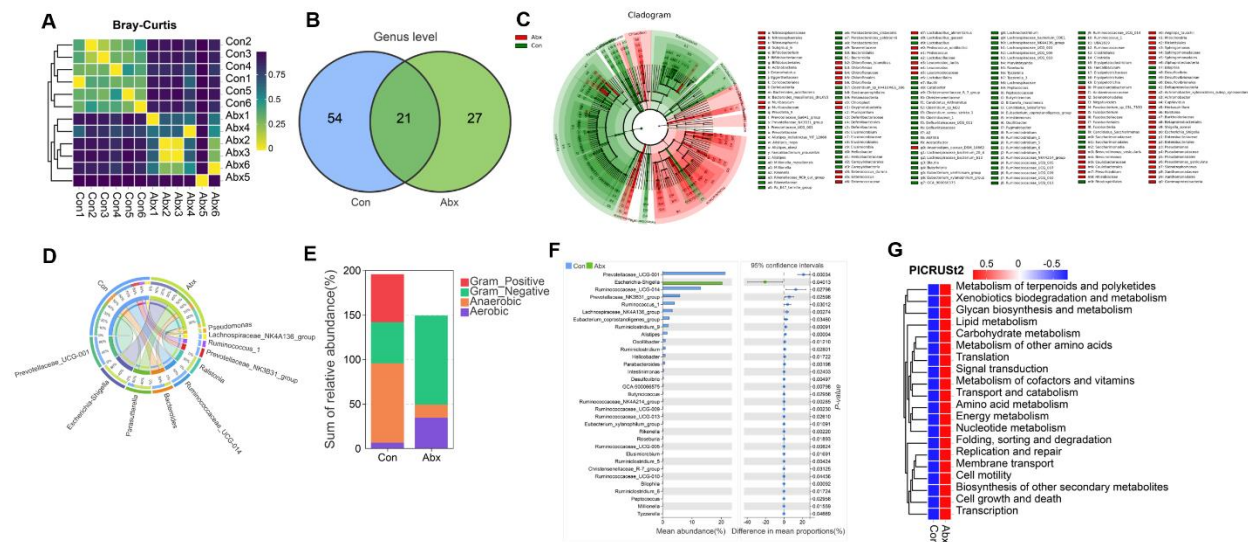


Figure S2. Microbial composition analysis for Abx group and Con group (related to Figure 1). **(A)** Pearson correlation heat map of 16S rRNA gene sequencing datasets showing microbial compositions in Abx group and Con group ($n = 6$ each). **(B)** Venn diagrams showing microbial compositions at genus level in Abx group and Con group. **(C)** LefSe depicting taxonomic association of microbial compositions between Abx group and Con group. Each circle on a different taxonomic level represents a species under that taxonomic level and the diameter of the circle is proportional to the relative abundance. **(D)** Circos diagram depicting microbial compositions at phylum level in Abx group and Con group. **(E)** The phenotypic distribution of each group analyzed by BugBase. **(F)** Welch's t test showing differences in species abundance for Abx group and Con group. **(G)** Functional analysis on the gut microbiome for Abx group and Con group using PICRUST2.

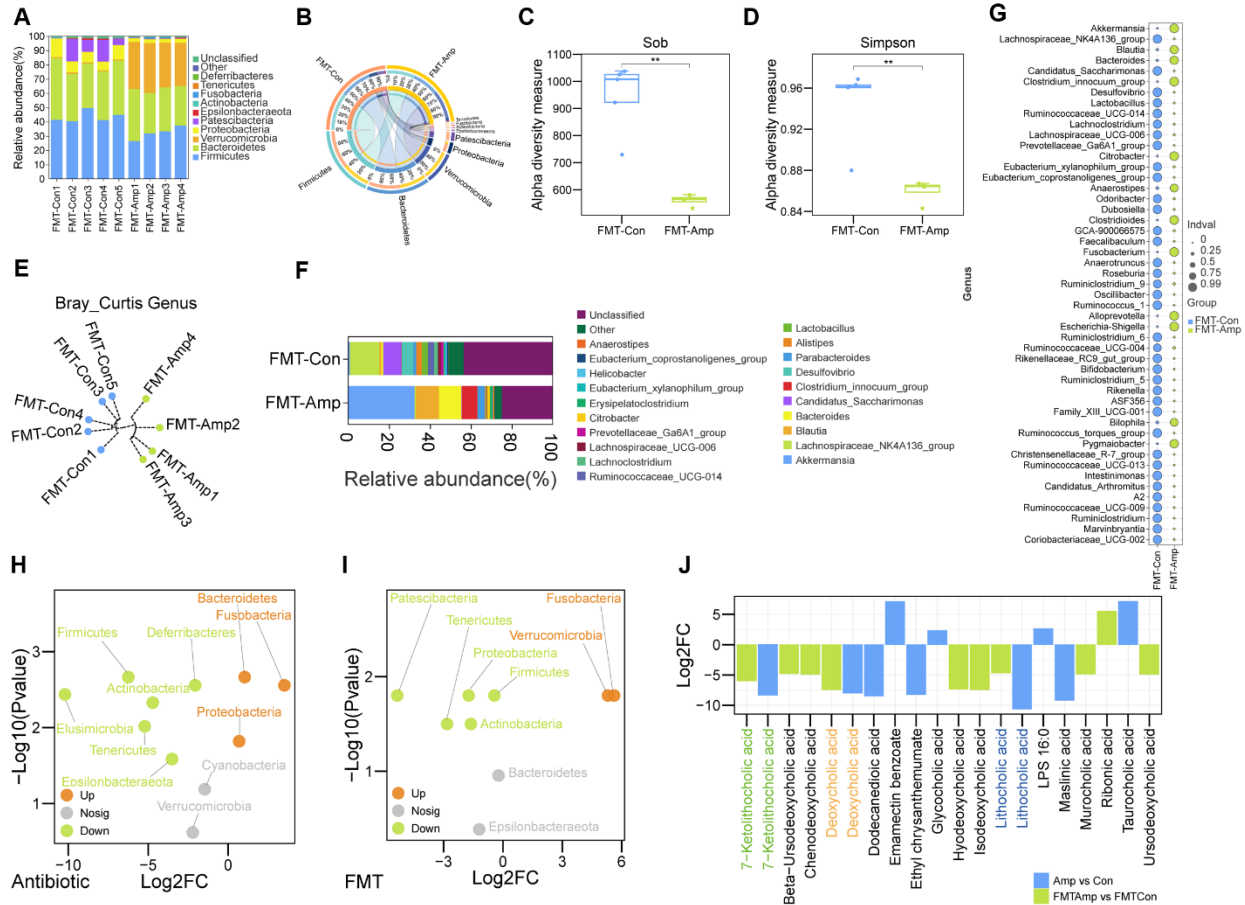


Figure S3. Microbial composition analysis after FMT experiments in germ-free mice (related to Figure 3). **(A)** Relative abundance of microbial compositions at phylum level in FMT-Amp group and FMT-Con group ($n = 4-5$ each). **(B)** Circos diagram depicting microbial compositions at phylum level in FMT-Amp group and FMT-Con group ($n = 4-5$ each). **(C)** Sob index showing alpha-diversity of microbial compositions in FMT-Amp group and FMT-Con group ($n = 4-5$ each). **(D)** Simpson index showing alpha-diversity of microbial compositions in FMT-Amp group and FMT-Con group ($n = 4-5$ each). **(E)** UPGMA analysis of microbial compositions at genus level in FMT-Amp group and FMT-Con group ($n = 4-5$ each). **(F)** Relative abundance of microbial compositions at genus level in FMT-Amp group and FMT-Con group ($n = 4-5$ each). **(G)** Indicator value analysis of microbial compositions at genus level in FMT-Amp group and FMT-Con group ($n = 4-5$ each). **(H)** Volcano plot showing up- and down-regulated microbiota at phylum level in Amp vs. Con comparison ($n = 6-7$ each). P value < 0.05 , measured with the unpaired, two-tailed Student's t test. **(I)** Volcano plot showing up- and down-regulated microbiota at phylum level in FMT-Amp vs. FMT-Con comparison ($n = 4-5$ each). P value < 0.05 , measured with the unpaired, two-tailed Student's t test. **(J)** Differential and common bile acids in Amp vs. Con comparison and FMT-Amp vs. FMT-Con comparison. Groups include control (FMT-Con) and ampicillin (FMT-Amp). $*P < 0.05$, $**P < 0.01$, $***P < 0.001$, $****P < 0.0001$, Student's t test.

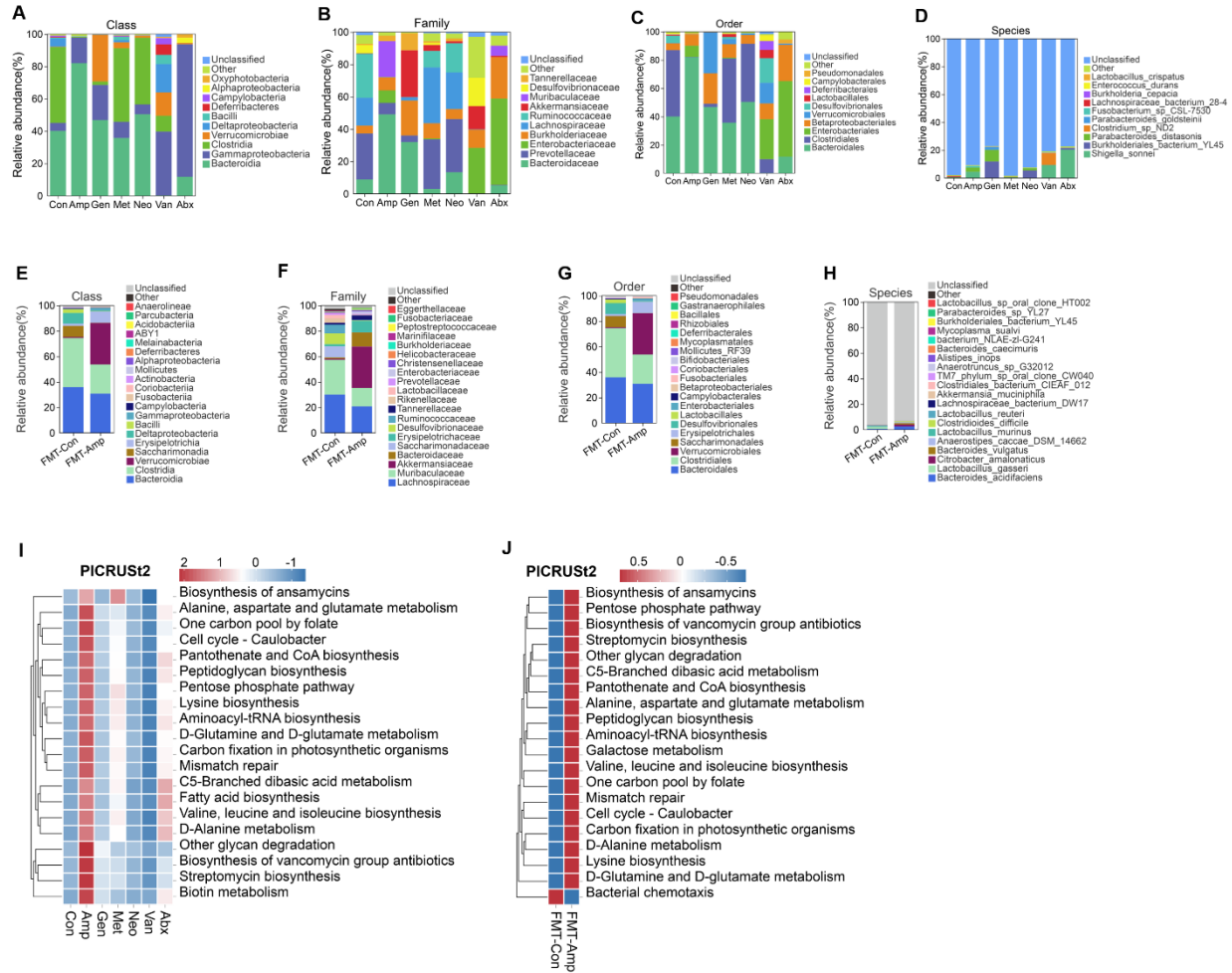


Figure S4. Microbial composition analysis at different levels (related to Figure 3). **(A-D)** Gut microbiota analysis of bacterial structure from SPF mice at class, family, order, species level, respectively ($n = 6-7$ each). Groups include control (Con), ampicillin (Amp), gentamicin (Gen), metronidazole (Met), neomycin (Neo), vancomycin (Van), antibiotic cocktail (Abx, mixture of the above five antibiotics). **(E-H)** Gut microbiota analysis of bacterial structure from GF mice at class, family, order, species level, respectively ($n = 4-5$ each). Groups include control (FMT-Con) and ampicillin (FMT-Amp). **(I)** Functional analysis on the gut microbiome for antibiotic-treated mice using PICRUSt2. **(J)** Functional analysis on the gut microbiome for FMT mice using PICRUSt2.

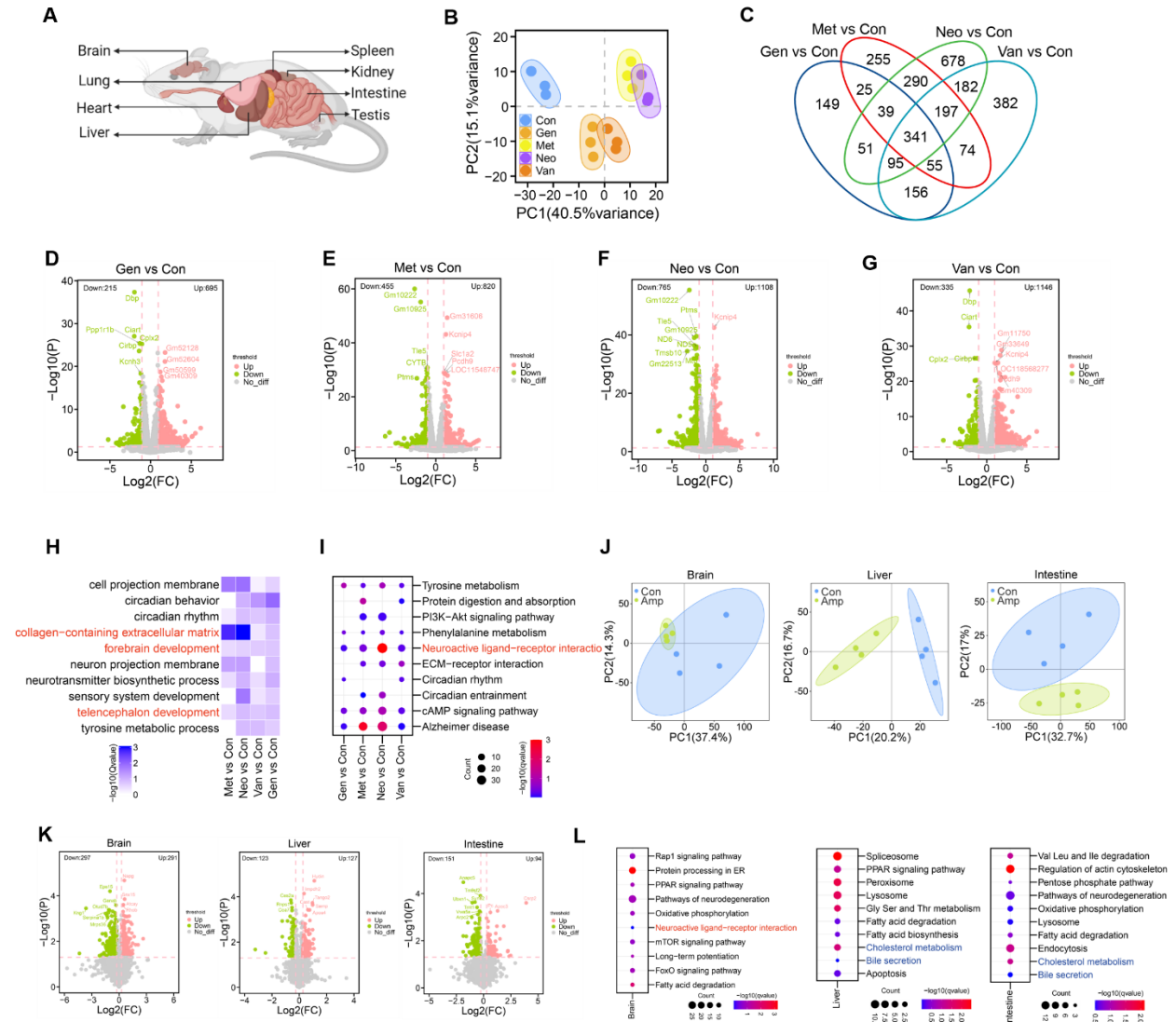


Figure S5. Transcriptome-wide impact of gut microbiota on brain gene expression (related to Figure 4). **(A)** Mouse model showing eight tissues from three groups (Con, Amp, Abx. $n = 3$ each) were collected for mRNA transcriptome sequencing. **(B)** PCA results of mouse brain mRNA transcriptome datasets in five groups (Con, Gen, Met, Neo, Van. $n = 3$ each). **(C)** Venn diagram showing the differences and overlaps of genes between groups ($n = 3$ each). **(D-G)** Volcano plot showing up- and down-regulated mouse brain genes in antibiotic treatment group compared to Con group ($n = 3$ each). Genes with expression level of fold change ≥ 2 and $P < 0.05$ are presented. **(H)** Gene Ontology analysis showing enriched pathways with differentially expressed genes in different groups compared to the control ($n = 3$ each). **(I)** KEGG analysis showing enriched pathways with differentially expressed genes in different groups compared to the control ($n = 3$ each). **(J)** PCA plot clustering mouse proteome datasets (brain, liver, intestine) between ampicillin treatment and the control ($n = 4$ each). **(K)** Differentially expressed proteins in proteome datasets (brain, liver, intestine) between ampicillin treatment and the control. Proteins with expression level of fold change ≥ 1.2 and $P < 0.05$ are presented. **(L)** KEGG analysis showing functional pathways of differentially expressed proteins in three tissues (brain, liver, intestine) by ampicillin treatment.

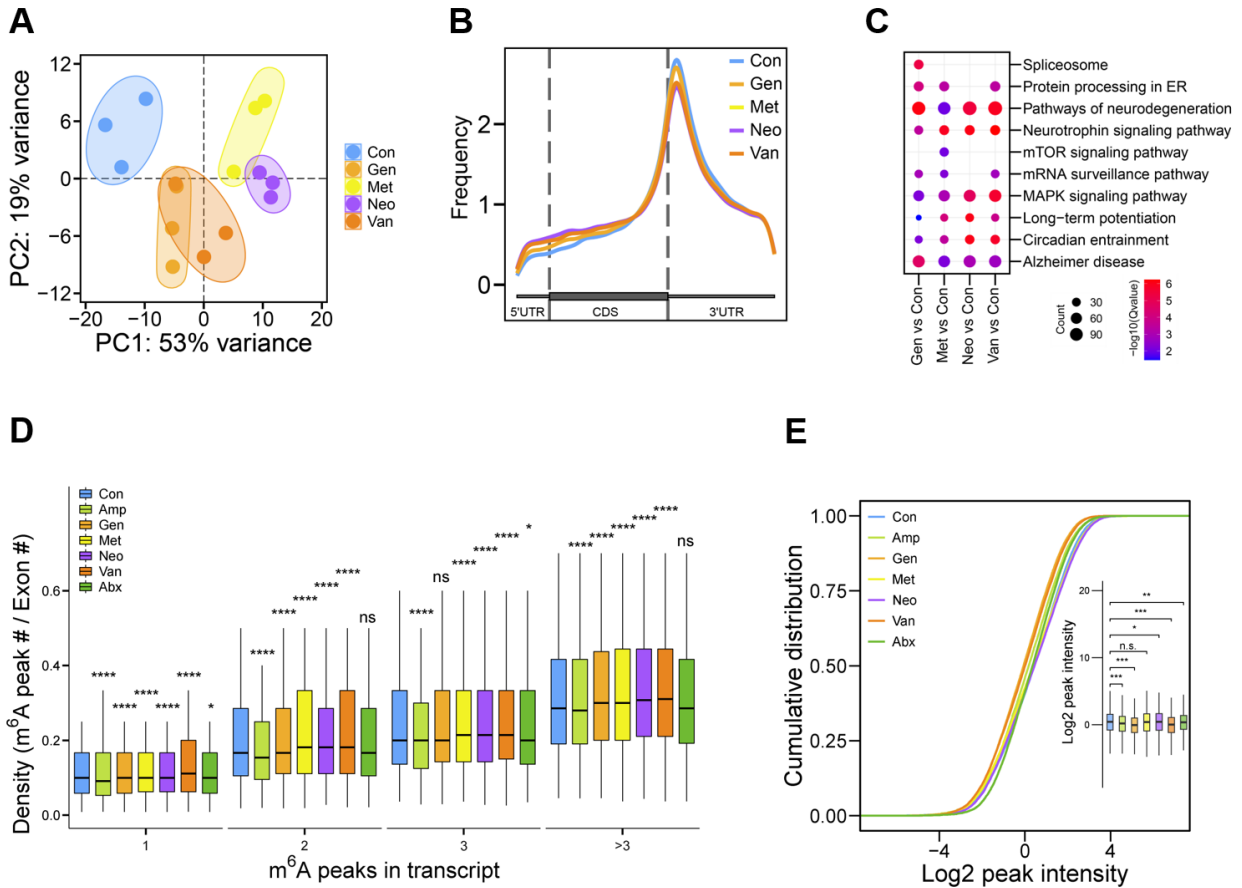


Figure S6. Gut dysbiosis rewrites host brain mRNA m^6A epitranscriptome and gene expression (related to Figure 5). (A) PCA results of mouse brain mRNA m^6A epitranscriptome datasets in different groups (Con, Gen, Met, Neo, Van. $n = 3$ each). (B) The frequency of m^6A peaks distributed across the mRNA regions (5'UTR, CDS, 3'UTR) in different groups ($n = 3$ each). (C) KEGG analysis showing functional pathways of differentially abundant m^6A peak-containing genes between different antibiotic-treatment groups and the control ($n = 3$ each). (D) Statistical analysis of m^6A peak/exon density in m^6A peak-containing genes between control and each of six antibiotic-treatment groups ($n = 3$ each). (E) Cumulative distribution of m^6A peak intensity in mouse brain of seven treatment groups ($n = 3$ each). * $P < 0.05$, ** $P < 0.01$, *** $P < 0.001$, **** $P < 0.0001$, Mann-Whitney-Wilcoxon Test.

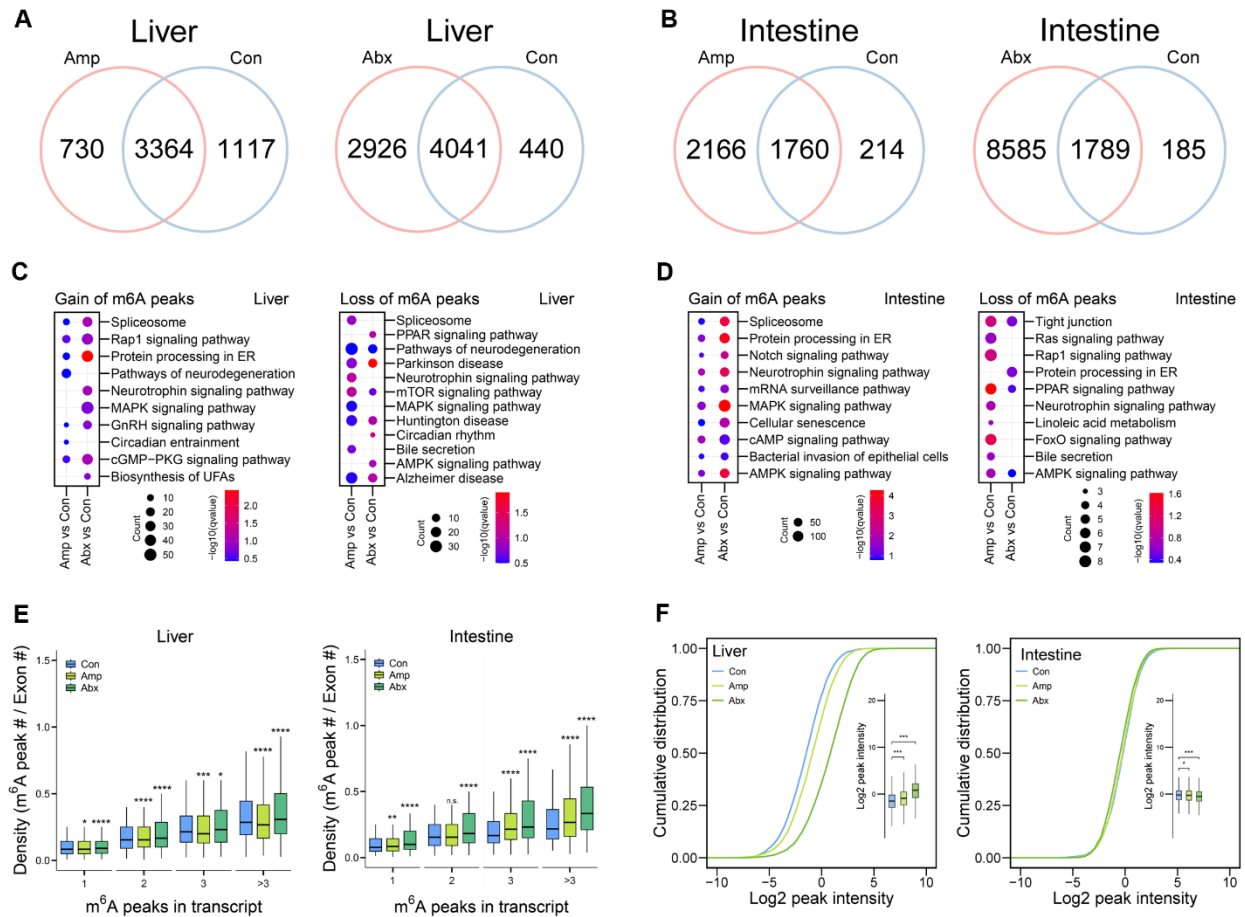


Figure S7. Gut dysbiosis rewrites host liver and intestine mRNA m⁶A epitranscriptome and gene expression (related to Figure 6). **(A)** The gain and loss peak numbers for the liver in three groups (Con, Amp, Abx. $n = 3$ each). **(B)** The gain and loss peak numbers for the intestine in three groups (Con, Amp, Abx. $n = 3$ each). **(C)** KEGG analysis showing pathways of liver genes gaining and losing m⁶A peaks in different groups ($n = 3$ each). **(D)** KEGG analysis showing pathways of intestine genes gaining and losing m⁶A peaks in different groups ($n = 3$ each). **(E)** Statistical analysis of m⁶A peak/exon density in m⁶A peak-containing genes (Con, Amp, Abx. $n = 3$ each). **(F)** Cumulative distribution of m⁶A peak intensity in seven groups (Con, Amp, Abx. $n = 3$ each). * $P < 0.05$, ** $P < 0.01$, *** $P < 0.001$, **** $P < 0.0001$, Mann-Whitney-Wilcoxon Test.

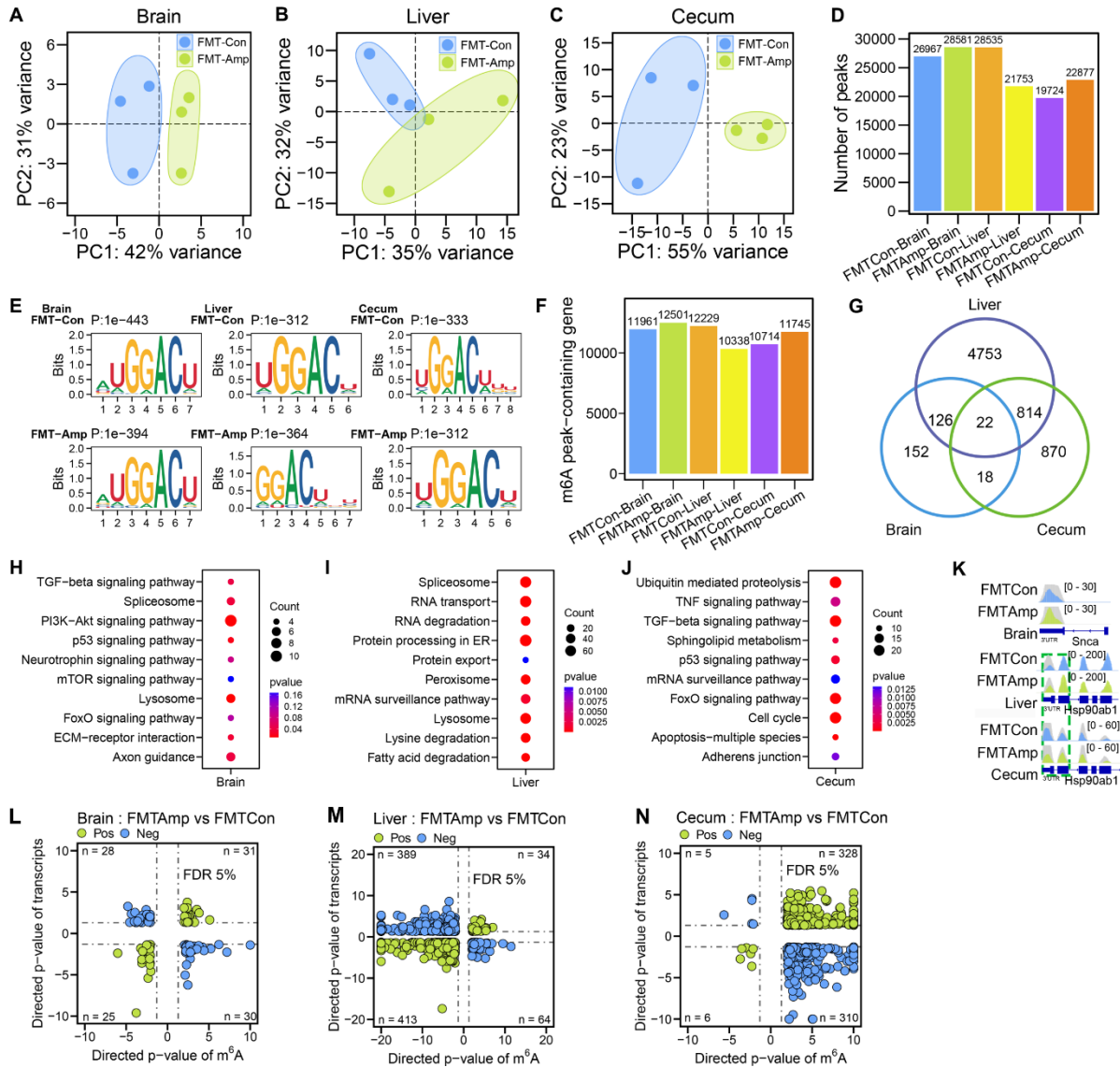


Figure S8. Gut dysbiosis reprograms host mRNA m^6A epitranscriptome in GF mice (related to Figure 6). (A-C) PCA plot clustering mRNA m^6A epitranscriptomes of three tissues (brain, liver, cecum) in FMT-Amp group and FMT-Con group ($n = 3$ each). (D) Numbers of peaks identified from brain, liver and cecum in two groups ($n = 3$ each). (E) Representative consensus motifs and corresponding P values of m^6A peaks identified from brain, liver and cecum in two groups ($n = 3$ each). (F) Numbers of m^6A peak-containing genes from brain, liver and cecum in two groups ($n = 3$ each). (G) Venn diagram showing the differences and overlaps of m^6A peak-containing genes between three tissues ($n = 3$ each). (H-J) KEGG analysis showing functional pathways of different m^6A peak-containing genes in three tissues (brain, liver, cecum, $n = 3$ each). (K) IGV depicting representative sequencing coverage of m^6A -IP (different colors) and Input (grey) showing differential m^6A peaks on transcripts *Snca* and *Hsp90ab1* in three tissues between two groups. (L-N) Correlation analysis of m^6A epitranscriptome with transcriptome in FMT-Amp compared to the control (brain, liver, cecum, $n = 3$ each).

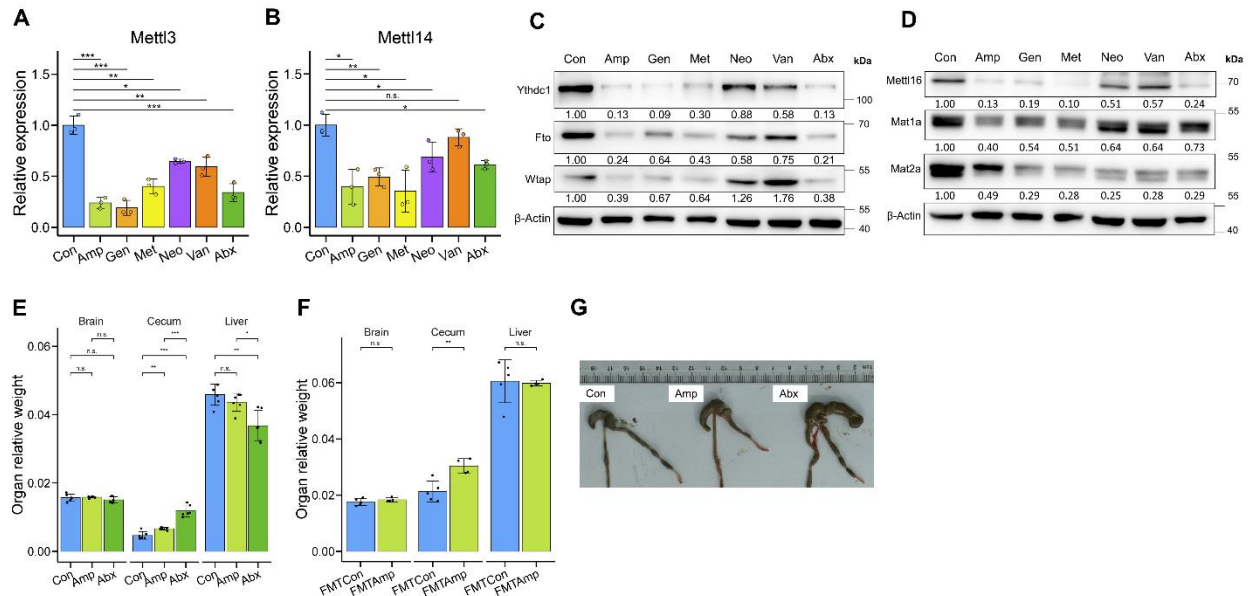


Figure S9. Gut dysbiosis regulates host m⁶A writers in mouse tissues and associated phenotypes (related to Figure 7). **(A)** Quantitative analysis of relative expression of METTL3 in brain from different antibiotic treatments (Con, Amp, Gen, Met, Neo, Van, Abx. *n* = 3 each). **(B)** Quantitative analysis of relative expression of METTL14 in brain from different antibiotic treatments (*n* = 3 each). **(C)** Western blot analysis of mRNA m⁶A machinery proteins (YTHDC1, FTO, WTAP) in brain from different antibiotic treatments, relative intensities of the proteins are indicated. **(D)** Western blot analysis of other methyl-donor related molecules (METTL16, MET1A, MET2A) in brain after antibiotic treatments, relative intensities of the proteins are indicated. **(E)** The organ relative weight of the tissues in mice after antibiotic treatments (*n* = 6). **(F)** The organ relative weight of the tissues in mice after FMT experiments (*n* = 4-5 each). **(G)** The images showing enlarged cecum tissue after antibiotic treatments. **P* < 0.05, ***P* < 0.01, ****P* < 0.001, *****P* < 0.0001, Student's t test.

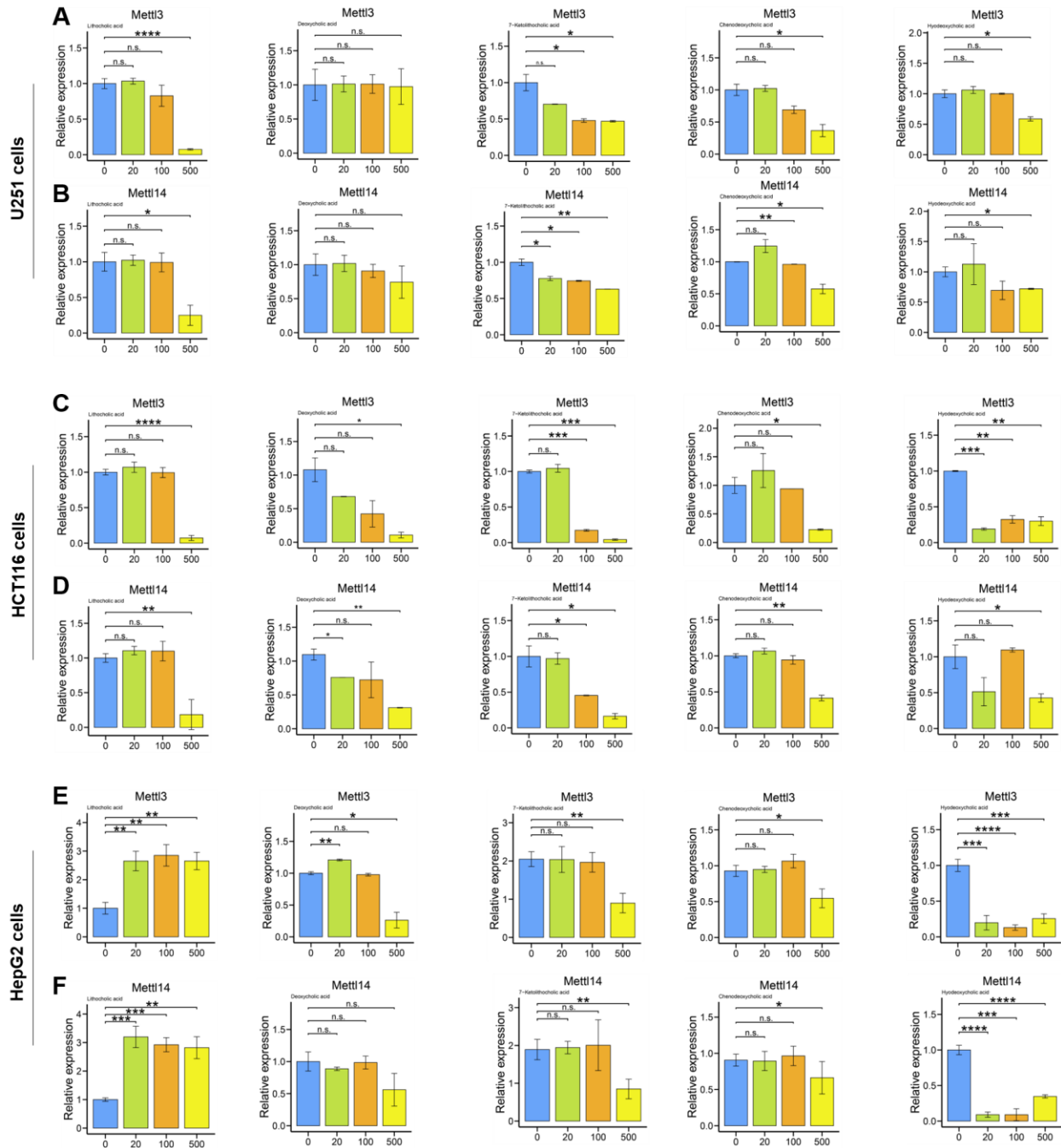


Figure S10. Bile acids treatments in mammalian cells alter the expression of m⁶A writers (related to Figure 8). (A, B) Quantitative analysis of relative expression of METTL3 and METTL14 in U251 cells treated with various concentrations of five different bile acids including lithocholic acid (*n* = 3), deoxycholic acid (*n* = 3), 7-ketolithocholic acid (*n* = 2), chenodeoxycholic acid (*n* = 2), and hyodeoxycholic acid (*n* = 2). (C, D) Quantitative analysis of relative expression of METTL3 and METTL14 in HCT116 cells treated with various concentrations of five different bile acids including lithocholic acid (*n* = 3), deoxycholic acid (*n* = 2), 7-ketolithocholic acid (*n* = 2), chenodeoxycholic acid (*n* = 2), and hyodeoxycholic acid (*n* = 2). (E, F) Quantitative analysis of relative expression of METTL3 and METTL14 in HepG2 cells treated with various concentrations of five different bile acids including lithocholic acid (*n* = 3), deoxycholic acid (*n* = 2), 7-ketolithocholic acid (*n* = 3), chenodeoxycholic acid (*n* = 2), and hyodeoxycholic acid (*n* = 3). **P* < 0.05, ***P* < 0.01, ****P* < 0.001, *****P* < 0.0001, Student's t test.